XIAOWEI FENG[1], FEI XUE[2*], XIAOTIAN FENG[3], TONGYANG ZHAO[2]

FAILURE CHARACTERISTICS OF W STRAP IN COAL MINE SUPPORT

W strap is a crucial surface support component for underground coal mine roadways. In this study, the failure characteristics of the W strap in the field are discussed, and the loading characteristics of the strap and the faceplate are numerically and experimentally analysed. Afterwards, a loading apparatus capable of reappearing the loading environment of the strap in the field is fabricated. This loading device, combined support systems consisting of a bolt, faceplate and strap is tested under different simulated strata conditions. Failure patterns of the strap are evaluated by the 3D scanning method, and proper selection of a faceplate is explored. Results indicate that a domed faceplate can achieve a favourable supporting effect on strata, and thus it is favoured compared with a square domed faceplate. In addition, rock cavity and rock integrity beneath the strap are essential factors determining the servicing life of the overall supporting system.

Keywords: W strap; field observation; laboratory tests; coal mine support; failure characteristics

1. Introduction

There are many selections for roadway supporting approaches in underground coal mines, such as standing supports, tendon supports and reinforcements, and surface restraint systems [1-4]. Among them, the W strap is a surface supporting component that can provide a sufficiently large holding force to the roadway roof. The strap can transfer the load from nearby rock mass to the yielding tendon, thereby improving the overall system performance considerably [5,6]. However, in most circumstances, they are weakened when applied in high in situ areas [1].

Relevant studies related to surface support elements, such as mesh and thin spray-on liners [7,8], are very popular [9-14]. Nonetheless, research related to the W strap has received little

---

[1]   CHINA UNIVERSITY OF MINING AND TECHNOLOGY, CHINA
[2]   SHAOXING UNIVERSITY, KEY LABORATORY OF ROCK MECHANICS AND GEOHAZARDS OF ZHEJIANG PROVINCE, CHINA
[3]   XI'AN UNIVERSITY OF ARCHITECTURE AND TECHNOLOGY, POLITECNICO DI MILANO, CHINA

*   Corresponding author: kdckxf@126.com
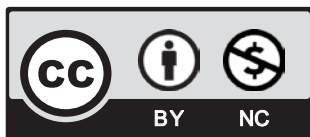
attention. The difference between wire meshes and W strap is apparent, even though both are pinned on the rock mass by tendons. Fig. 1 shows the comparison of the supporting effects for different types. The advantages of the supporting pattern of section I are apparent, the load can spread through the entire strap, and a potential weak bolting point can be strengthened by neighbouring strong bolting units. A supporting configuration like this is very effective, especially for sites that have suffered overly large stress concentrations [15].

In this study, research is conducted to understand the mechanical properties of the W strap, and its cooperation effects with assembled components are also discussed, with the hope of deepening the understanding of the mechanical responses of the strap and providing particular references for the practitioners.
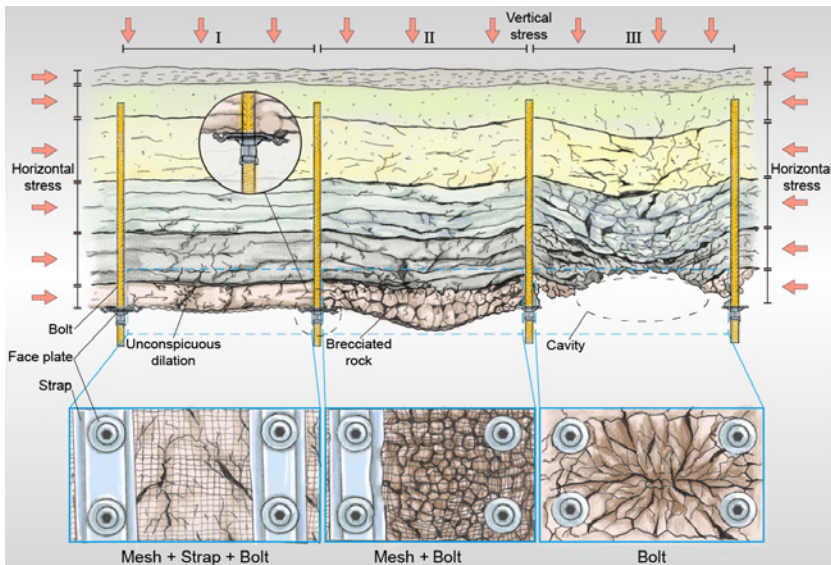

Fig. 1. Supporting effects comparison for a bolt, a mesh+bolt, and a mesh+strap+bolt

2. Field observation

2.1. General distortion of the W strap

Failure patterns of W strap in the engineering field are exemplified in Fig. 2. The supporting pattern consisted of rock bolts, cable bolts, W straps, meshes, and faceplates, which is a conventional supporting pattern. The strap distortion can be classified as either an S-shaped fold, Z-shaped fold, V-shaped fold, inverted V fold, or multiple folds. These distortion types are representative, as all types of strap distortions in the field can match their type to a specific form in the figure.

Detailed breakage patterns of the strap-bolt supporting system are shown in Fig. 3. In summary, the rupture of the rock bolt, decoupling, and the rupture of the cable bolt are typical failure patterns for the bolting unit[16], thereby leaving either indentation or shearing through (sinking) on the strap.
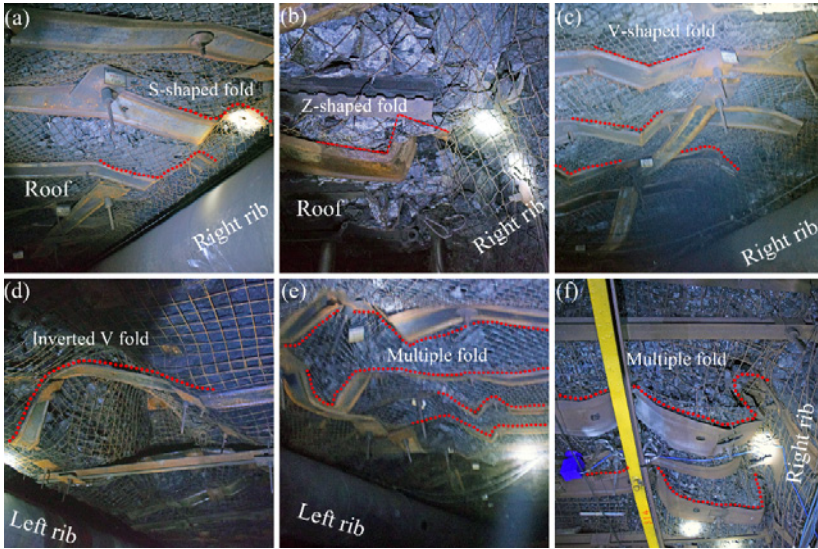
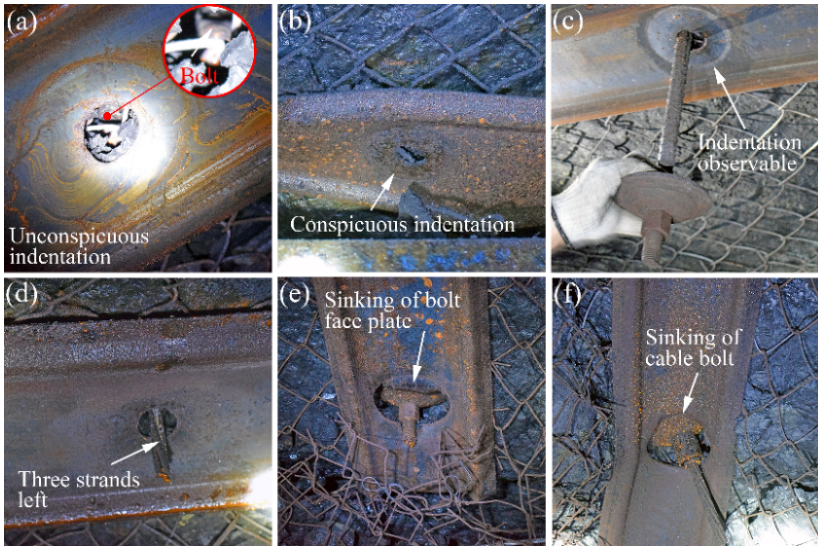Fig. 2. Overall distortions of W straps based on in situ observations

Fig. 3. Detailed failure patterns of the strap-bolt supporting system

2.2. Numerical simulation of different face plates

The faceplate installed on the strap normally can have two types, dome-shaped with no flat wing around the dome (referred to as a domed faceplate, DFP), square domed with a square flat wing jointed to the domed part (referred to as a square domed faceplate, SDFP). Numerical

calibration (ABAQUS) was carried out to analyse the mechanical coupling of the faceplate and strap (Fig. 4i). Solid element C3D8R was adopted for the modelling of all components. The size of the DFP was 120 mm in diameter, 10 mm in thickness and 25 mm in height. The size of the SDFP was 120 mm in diameter, 10 mm in thickness, 80 mm in diameter for the domed part, and 25 mm in height. All the above dimensions mirrored that of the actual components. The loading source was a cylindrical rigid body, and the degrees of freedom were all restrained. The base was simulated with an ideal elastic material associated with an elastic modulus and Poisson's ratio of 25000 N/mm^2 and 0.2, respectively. The bottom surface of the base was fixed with all the degrees of freedom restrained. Moreover, normal hard contact and tangent Coulomb friction were adopted to simulate the contact property between the surfaces of the components. The loading was controlled by a maximum loading downward stroke of 15 mm.

Figs. 4a-b present the stress fields on the base of SDFP configuration at different loading strokes, the diameter of the ring-like stress pattern is just the same as the diameter of the domed part of SDFP when the stroke is 6.75 mm. When the stroke reaches 15 mm, the ring splits into four sections because of the overlarge stress concentration at the edge of the domed part due to the corners warp. Stress patterns in Figs. 4f-h further demonstrates that the domed part of the SDFP is the core for mechanical performance, and the flat section can not provide enough support, especially after the corners warp.
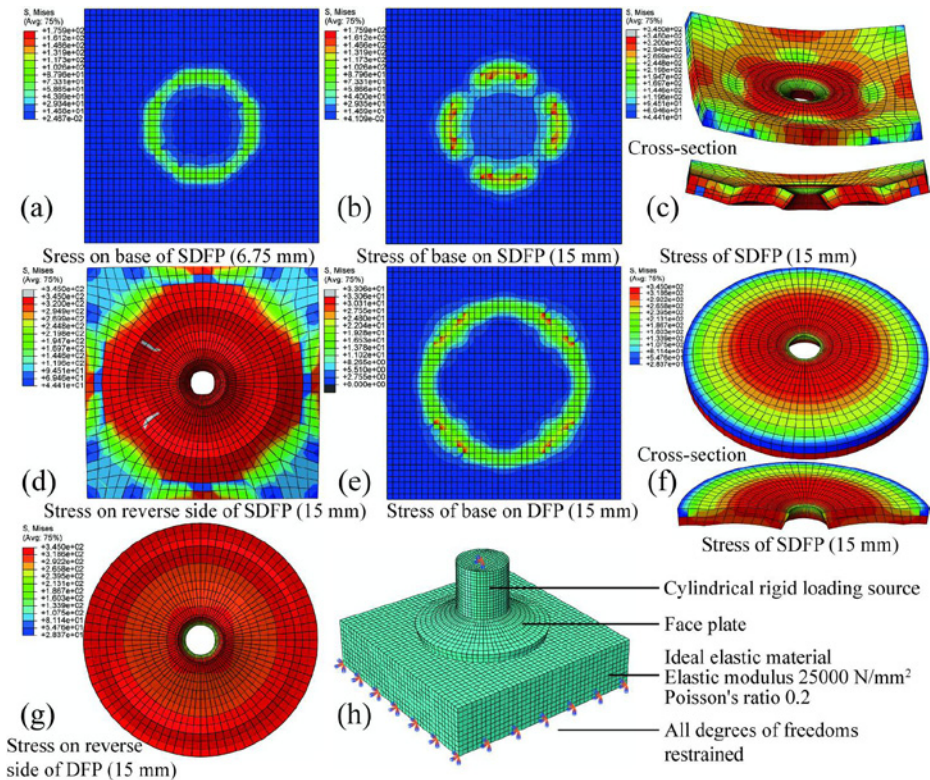

Fig. 4. Numerical simulation results for the square domed face plate and domed face plate

In Fig. 4e, the stress distribution on the base of DFP is exhibited, a vivid ring-like concentration area can be seen, and the diameter is also the same as the diameter of DFP, indicating that the circular edge of DFP is pivotal for loading and transferring. The maximum stress here is lower than that of the SDFP configuration (Fig. 4b) since the load is distributed on a relatively larger 'ring', and the incurred stress will decrease accordingly. The stress pattern on DFP at the end of the stroke (15 mm) also demonstrates an inside-out transferring process, the stress decreases as the distance to the hole centre increases (Figs. 4f-h), and the centre part plays a key role here.

Given the above results, the mechanical behaviour of the DFP configuration, under the numerical simulation setting, can be better than that of the SDFP configuration under identical predefined deformation values.

2.3. Compression test on different face plates

Laboratory compression tests on the faceplates are shown in Fig. 5a. Both stiffness and the peak load for the DFP are much larger than the SDFP. The peak force for the DFP is 369.49 kN, which is 2.78 times the peak load (132.71 kN) of the SDFP. In Fig. 5b, the failure patterns are presented. Warping of the corners is shown for the SDFP, and this phenomenon conforms with the numerical results. Overall, the mechanical property of the SDFP is mainly determined by the outer edge of the domed part. For the DFP, the outer edge is the load bearing ring before the failure.
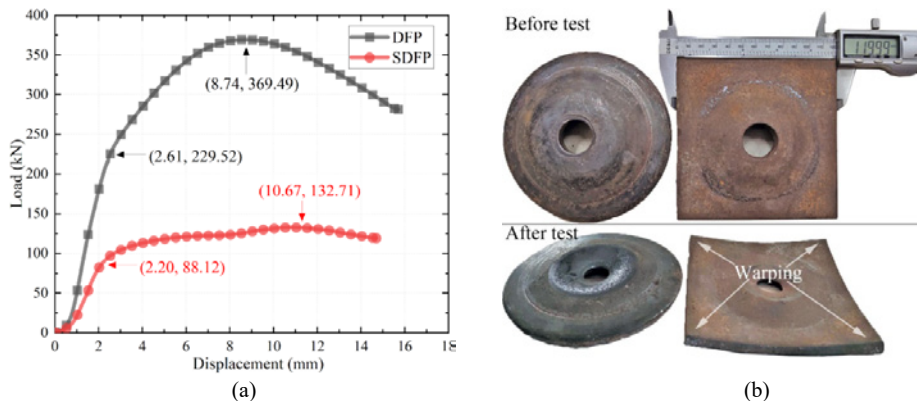

Fig. 5. Compression test results on the domed face plate and square domed face plate

3. Loading patterns

Schematic drawing of the loading equipment for the bolt-strap system is presented in Fig. 6.

The preparation process and the testing process are shown in Fig. 7. Firstly, the cement blocks are prepared to simulate the blocky roof strata (Fig. 7a). Secondly, gravels with a diameter ranging from 10 mm to 30 mm are paved on the top of the cement blocks, and the overall thickness is 50 mm (Fig. 7b). Thirdly, the W strap is placed in the loading box, and then the faceplate and the nut are installed accordingly (Fig. 7c). Finally, the entire system is transferred to the MTS machine for loading (Fig. 7d). The bolt is 18 mm in diameter and 50 cm in length, and the strap
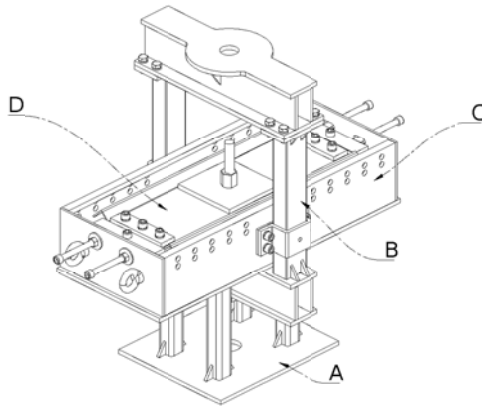
Fig. 6 Schematic drawings of the loading equipment, pedestal (A), loading frame (B), loading box (C), strap and affiliated components (D)

is 50 cm in length, 25 cm in width, and 3 mm in thickness. The faceplate was a domed type (DFP), with a 120 mm diameter and a thickness of 10 mm. The mechanical behaviour of the strap is greatly influenced by the cracks and caved holes beneath it. Three scenarios have been proposed and presented in Fig. 8.
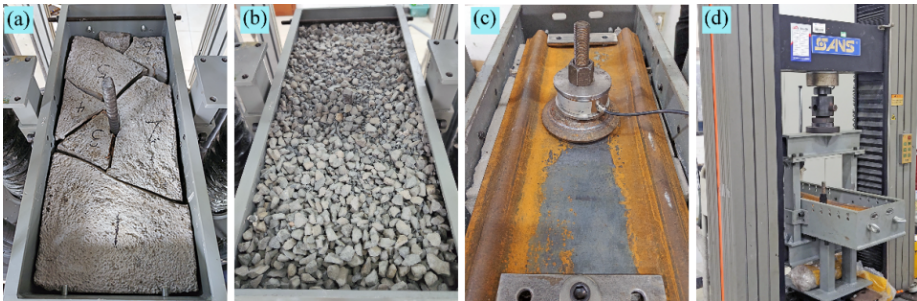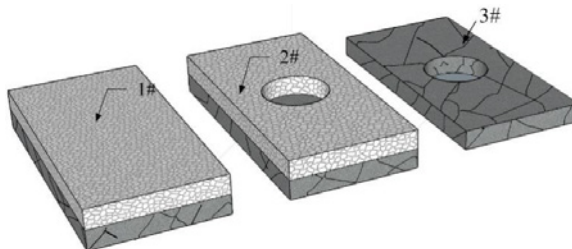

Fig. 7. Preparation procedure of testing system

Fig. 8. Simulated roof types. 1) Cracked high-strength concrete blocks were overlaid by a gravelsled layer. 2) A circular hole with a diameter of 150 mm was reserved in the centre of the upper layer (gravelsled layer). 3) A circular hole with a diameter of 150 mm was reserved at the centre of the concrete layer.

4. Results and analysis

4.1. Mechanical analysis

Testing configurations were labelled as configurations #1, #2 and #3 in accordance with the patterns in Fig. 8. The loading rate is set as 10 mm/min, and then the results are plotted in Fig. 9a. The peak loads and displacements at the peak for configurations #1, #2 and #3 are 128.62 kN, 23.47 mm, 145.78 kN and 40.22 mm, and 140.43 kN and 67.67 mm, respectively, and the stiffness is plotted in Fig. 9b. For configuration #1, since the gravelled layer is compact, the buckling of the strap can be avoided, and the bearing capacity of the system is more likely to be determined by the strength of the bolt, faceplate, or nut. This result is supported by field observations where some supporting systems failed with a bolt rupture while the affiliated components were undamaged, as shown in Fig. 3a.
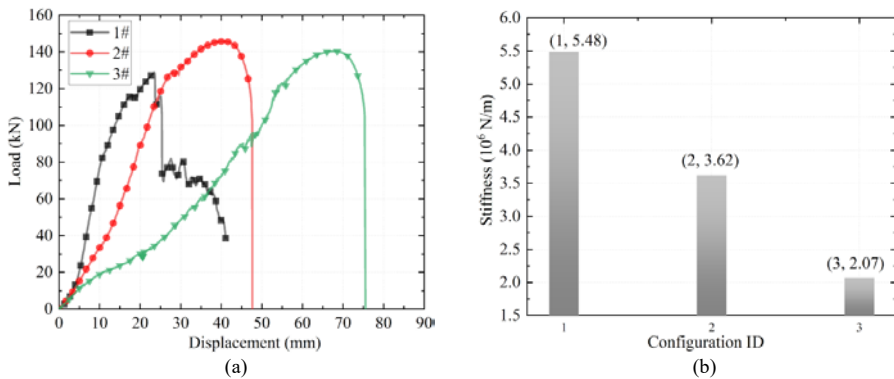

Fig. 9. (a) Load-displacement relationship for configuration #1~#3,
(b) stiffness decreasing trend for configuration #1~#3

The inner wall of the circular hole in configuration #2 is not stable because it was constructed with gravel which will collapse under loading. Therefore, a relatively small stiffness is expressed, or an apparent sinking of the faceplate is observable. For configuration #3, it is unlikely for the inner concrete wall of the circular hole to collapse. The stiffness of the system is even smaller because the sinking and shearing of the faceplate are the main factors that should be considered.

4.2. Deformation analysis

Fig. 10 lists the eventual failure patterns for all specimens. All tests are terminated by bolt rupture. The faceplates barely express the deformation and no distortion can be observed since the maximum loading to deformation of the faceplate is 369.5 kN (Fig. 5a), which is much higher than the peak values in Fig. 9a. Regarding the distortion of the strap, the strap in configuration #1 exhibits the smallest distortion, and only some small-scale bend can be seen (see Fig. 10a). The shearing stress on the concentration ring of the faceplate is co-sustained by the gravel and the strap. Fig .10b shows an indentation on the strap.

For configuration #2, the strap distortion becomes apparent (Fig. 10c). The pre-prepared hole beneath the centre hole of the strap amplifies the shearing role (sinking) of the faceplate. However, a collapse of the hole is unavoidable, thus diminishing the shearing stroke of the faceplate and alleviating the strap distortion. For configuration #3, the inner wall will not collapse if the load is appropriate. Then, the shearing stroke will not be diminished, eventually leading to even more apparent distortion of the strap, as seen in Fig. 10d.
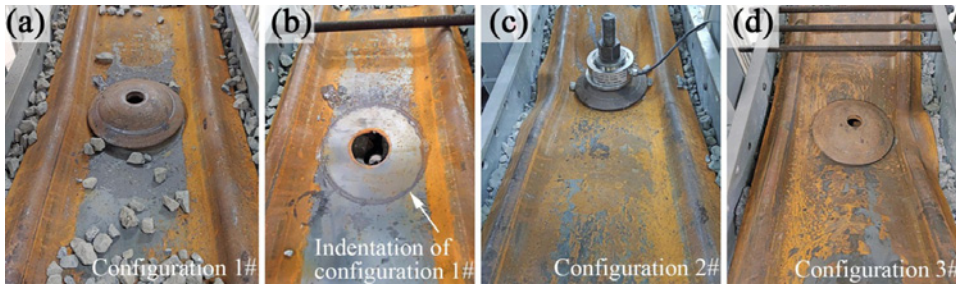

Fig. 10. Distortion patterns for straps

3D scanning was conducted for the purpose of detailed measurement of the strap deformation. The cloud maps are shown in Fig. 11a-c, through which the surface elevation at different points on the strap can be viewed and judged.

For configuration #1 (Fig. 11a), the distortion field has a good symmetry property, and the deep blue area indicates the indentation scope due to compression of the faceplate. Overall, the distortion looks similar to the V-shaped fold proposed in Fig. 2. For configuration #2, the left section has a comparatively intense distortion, while the distortion in the right section is relatively gentle. The large scope of the blue areas in Fig. 11b indicates a high degree of sinking due to the shearing of the faceplate. For configuration #3, the V-shaped fold distortion is more apparent (Fig. 11c). The deep blue area indicating a sink is roughly rectangular-shaped, and the spreading scope is limited because the inner wall of the reserved hole is unlikely to collapse. The distortion degree is the highest in all configurations.

4.3. Extended test on the square domed face plate

The mechanical behaviours of the SDFP and DFP are compared in this section. The configuration is the same as the No. 3 in Fig. 8, the dimensions of the SDFP are 120*120 mm in edge length and 10 mm thick. All of the loading conditions are unchanged. The testing results are shown in Fig. 12. The peak load and the displacement at the peak for the SDFP and DFP are 117.77 kN-39.22 mm and 146.97 kN-38.84 mm, respectively, and the stiffness for the SDFP and DFP are $3.00*10^6$ N/m and $3.78*10^6$ N/m, respectively. The above result proves that the DFP has a higher strength. The loading relationship for the DFP configuration is very similar to the bolt tensile curve, as can be revealed by the yield stage, hardening stage, and necking stage. The mechanical response is comprehensively dependent on the tensile behaviour of the bolt and the sinking of the faceplate.
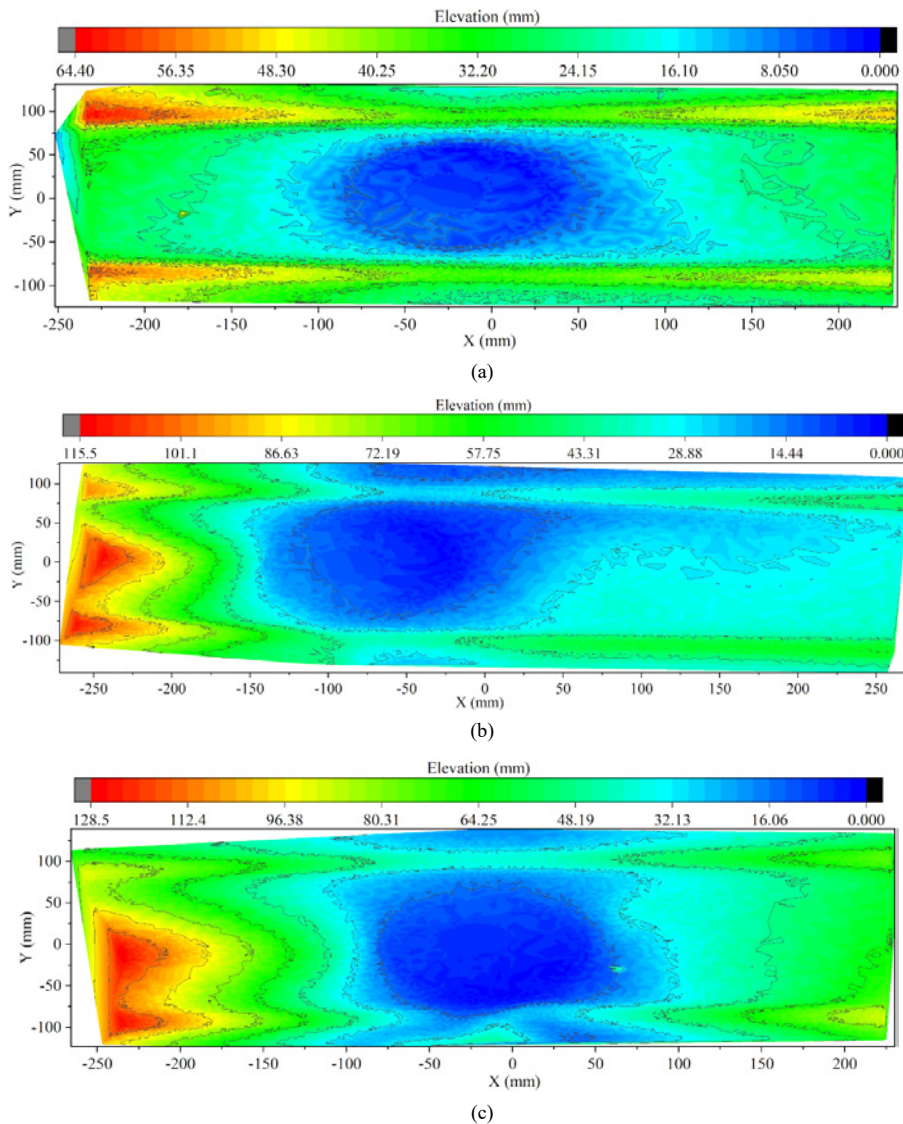
Fig. 11. Cloud maps for deformed straps in configuration #1~#3

The strap distortion of the SDFP configuration is not very severe when compared with that of the DFP configuration (Fig. 13a-b). The middle right section of the strap for the DFP configuration is extremely warped. A sharp crack is noticed in the strap of the SDFP configuration (Fig. 13a). The crack was caused by squeezing the nut when the faceplate was reversely deformed (Fig. 13d). The pattern before the test is shown in Fig. 13c. The reverse side of the SDFP is appended in Fig. 13e, where cracks can also be seen. The morphology of the concrete hole beneath the strap after the test is shown in Fig. 13f.
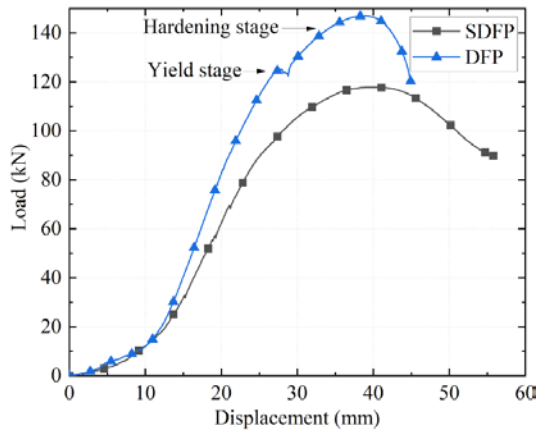
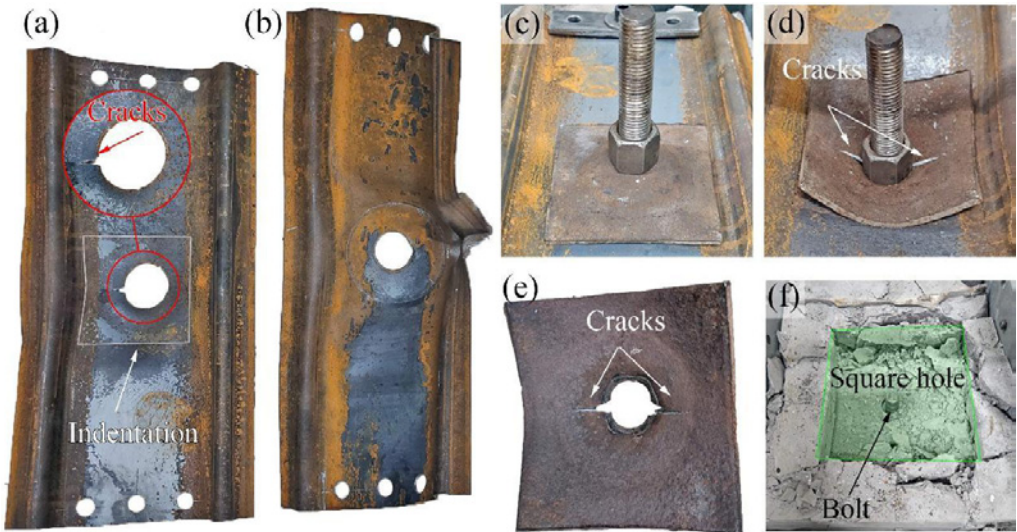Fig. 12. Displacement-load relationship for a DFP and SDFP configuration

Fig. 13. Test photos for the SDFP and DFP configuration. Strap distortion of the SDFP configuration (a) and the DFP configuration (b), (c) SDFP configuration before the test, (d) failure pattern of the SDFP configuration after the test, (e) wrong side of the SDFP after the test, (f) breakage pattern of the simulated square hole after the test

A cloud diagram revealing the surface elevation of the strap in the SDFP configuration is shown in Fig. 14. In Fig. 14a, most areas on the surface of the strap express no apparent distortion, the centre area behaves with the lowest elevation, and the outer contour line in this area is quite similar to the size of the square domed faceplate. To be more specific, the oval-shaped blue area at the centre indicates a severe sinking and is influenced by the sinking of the nut at a later stage.
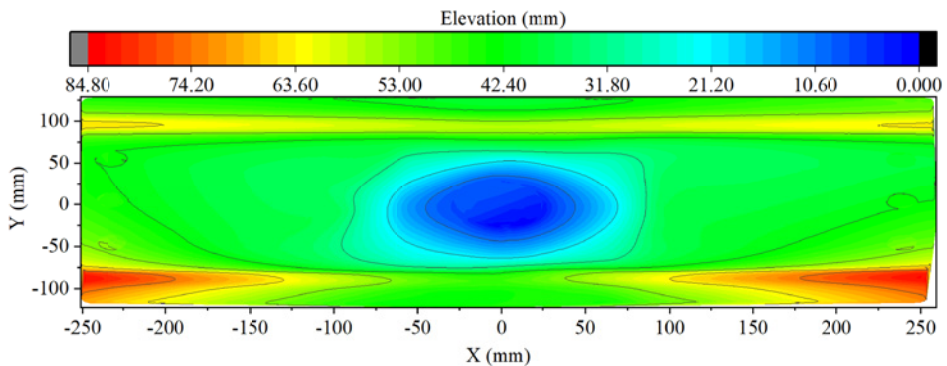
Fig. 14. Scanned cloud view of strap distortion in the SDFP configuration

4.4. Impacts of strap thickness

The above test utilised the strap with a thickness of 3 mm. To better understand the impacts of the strap thickness on its mechanical characteristics, a numerical simulation was conducted by ABAQUS. Models of straps with a thickness of 1 mm, 3 mm and 5 mm were constructed. Following the same dimensions as the actual ones, the strap was placed on a rigid platform, and a circular hole was opened on the platform where the hole of the strap existed. All components were simulated by the S4R element and the fixed boundary parts were simplified as a rigid body with all degrees of freedom restrained. Then a maximum load of 200 kN was applied on the face-plate, by which the strap was pressed to simulate the engineering scenario. The model of normal hard contact and tangent Coulomb friction was adopted to simulate the interaction between the contact surface of the components.

The results are listed in Fig. 15 and show that the 1 mm strap failed when the load reached 100 kN. The left three cloud maps are deformation changing fields for straps with a thickness of 1 mm, 3 mm and 5 mm, respectively. The deformation values were comparatively conservative compared with the experimental scenario. It was mainly due to the boundary conditions of the numerical model that could be more precisely controlled. When the strap thickness is 1 mm, the upward warp at the lower flanks can be seen, and the maximum value is 19.97 mm. For a 3 mm and 5 mm strap, no apparent warp can be noticed, and an insignificant difference can be seen between them, considering the deformation values were at different parts.

The right three cloud maps in Fig. 15 are stress changing fields for the straps. The stress distribution of the 1 mm strap can be more extensive, buckling and stress concentration are observable, and it failed at 100 kN. Comparing the 3 mm and 5 mm strap, the stress patterns at a 200 kN loading indicate that the 3 mm strap can be more sensitive in transmitting stress to its flanks and the loading circle is more influential, and the overall lower stress on the 5 mm strap demonstrates more favourable reliability. Nonetheless, the 3 mm thickness strap can satisfy the supporting effects considering the material cost and mechanical characteristics at the same time. Therefore, a 3 mm strap is a reasonable selection for coal mine support if the maximum load on the faceplate is lower than 200 kN, and a 4 mm or 5 mm W strap should be more acceptable if the rock stability diminishes.
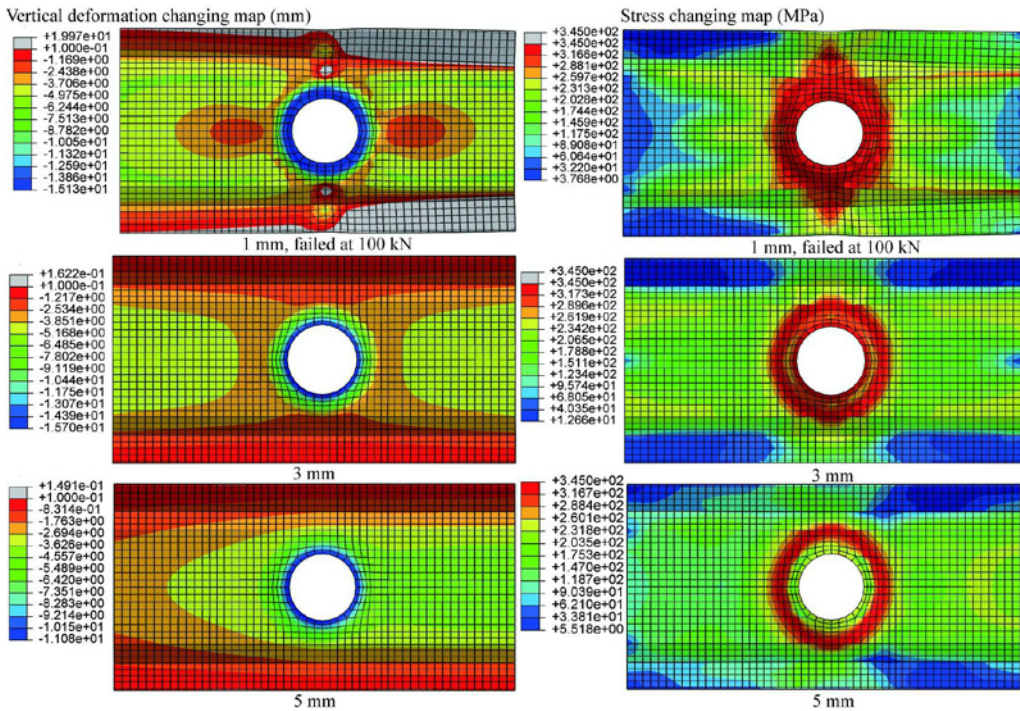
Fig. 15. Mechanical responses of straps with different thickness based on numerical simulation

5. Brief discussion

Perceptually speaking, practitioners can believe that SDFP is better for support since the flat wing can be useful to disperse the stress and thus enlarge the supporting area to rock mass. Nowadays in most coal mines in China, SDFP selection is more common compared with DFP selection. However, our numerical simulation and experimental analysis indicate that the mechanical performance of DFP can be significantly better than that of SDFP, and the loading capacity of SDFP is depleted by the corners warping under the high axial force of the bolt. Though the shearing strap failure due to concentrated stress at the edge of DFP can be common in the engineering field, it is still believed that the load before the failure can be favourable compared with the SDFP scenario. In the future, the relationship between stress corrosion and the humidity at the contacting face between the faceplate and strap should be investigated to deepen our understanding of this problem.

6. Conclusions

(1) The failure characteristics of W straps were analysed based on field observations. These types are representative and can correspond with most of the in situ failure patterns of the straps. The stress interaction relationship between the DFP (SDFP) and the strap is

revealed. The function of the flat wing of SDFP is normally weak in transferring stress due to wing warping.

(2) A loading apparatus was designed for reappearing the loading environment of the strap in the field. The distortion characteristics of the strap were analysed, and the results indicated that fragmented rock might not be detrimental to the distortion of the strap. If a rigid cavity exists beneath the strap and the faceplate only presses the cavity, distortion could occur immediately.

(3) The warping of the SDFP could deplete the bearing capacity of the faceplate, but the favourable anti-warping capacity of the domed faceplate was able to create a higher bearing state as long as the rock mass beneath it was intact.

(4) Additional numerical simulation indicates that a strap with 3 mm thickness is a proper selection, and favourable supporting effects can be obtained when it cooperates with DFP. The shearing strap failure due to the DFP edge should be discussed further by considering the influence of stress corrosion and humidity.

Acknowledgements

References

[1]   J.M. Galvin, Ground Engineering - Principles and Practices for Underground Coal Mining. Springer International Publishing (2016).

[2]   S. Nakamoto, N. Iwasa, J. Takemura, Effects of nails and facing plates on seismic slope response and failure. Géotechnique Letters 7 (2), 136-145 (2017). DOI: https://doi.org/10.1680/jgele.16.00179

[3]   C.C. Li, Principles of rockbolting design, Journal of Rock Mechanics and Geotechnical Engineering 9 (3), 396-414 (2017). DOI: https://doi.org/10.1016/j.jrmge.2017.04.002

[4]   X. Feng, N. Zhang, F. Xue, Z. Xie, Practices, experience, and lessons learned based on field observations of support failures in some Chinese coal mines. International Journal of Rock Mechanics and Mining Sciences 123, 104097 (2019). DOI: https://doi.org/10.1016/j.ijrmms.2019.104097

[5]   B.P. Simser, Rockburst management in Canadian hard rock mines. Journal of Rock Mechanics and Geotechnical Engineering 11 (5), 1036-1043 (2019). DOI: https://doi.org/10.1016/j.jrmge.2019.07.005

[6]   C. Wei, C. Zhang, I. Canbulat, A. Cao, L. Dou, Evaluation of current coal burst control techniques and development of a coal burst management framework. Tunnelling and Underground Space Technology 81, 129-143 (2018). DOI: https://doi.org/10.1016/j.tust.2018.07.008

[7]   Z. Shan, I. Porter, J. Nemcik, E. Baafi, Beam enhancement capacity of a thin fibre-reinforced polymer liner. Géotechnique Letters 10 (4), 478-485 (2020). DOI: https://doi.org/10.1680/jgele.19.00112

[8]   Q. Qiao, J. Nemcik, I. Porter, E. Baafi, Laboratory investigation of support mechanism of thin spray-on liner for pillar reinforcement. Géotechnique Letters 4 (4), 317-321 (2014). DOI: https://doi.org/10.1680/geolett.14.00076

[9]   H. Yilmaz, Development of testing methods for comparative assessment of thin spray-on liner (TSL) shear and tensile properties, University of the Witwatersrand, South Africa (2011).

[10] A. Spearing, J. Ohler, E. Attiogbe, The effective testing of thin spray-on liners (superskins) for use in underground mines. In: Surface support in mining. Y. Potvin, T. Stacey, J. Hadjigeorgiou, editors. Nedlands: Australian centre for Geomechanics, pp. 97-102 (2004).

[11] E. Villaescusa, Weld mesh for static rock support in Australia. In: Surface support in mining. Y. Potvin, T. Stacey, J. Hadjigeorgiou, editors. Nedlands: Australian Centre for Geomechanics 385-390 (2004).

[12] J. Nemcik, I. Porter, E. Baafi, C. Lukey, Geotechnical assessment of skin reinforcement in underground mines. In: Proceedings of 28th international conference on ground control in mining Morgantown 256-260 (2009).

[13] Z. Shan, I. Porter, J. Nemcik, E. Baafi, Investigating the behaviour of fibre reinforced polymers and steel mesh when supporting coal mine roof strata subject to buckling. Rock Mechanics and Rock Engineering **52** (6), 1857-1869 (2019). DOI: https://doi.org/10.1007/s00603-018-1656-1

[14] Z. Shan, P. Ian, N. Jan, B. Ernest, S.O. Civil, Comparing the reinforcement capacity of welded steel mesh and a thin spray-on liner using large scale laboratory tests. International Journal of Mining Science and Technology **24** (3), 373-377 (2014). DOI: https://doi.org/10.1016/j.ijmst.2014.03.015

[15] R. Frith, G. Reed, M. McKinnon, Fundamental principles of an effective reinforcing roof bolting strategy in horizontally layered roof strata and areas of potential improvement. International Journal of Mining Science and Technology **28** (1), 67-77 (2018). DOI: https://doi.org/10.1016/j.ijmst.2017.11.011

[16] Y. Zhang, Y. Jiang, C. Wang, M. Chen, Q. Yin, Shear of bolted non-persistent joints: role of bolting conditions and joint persistency. Géotechnique Letters **10** (4), 550-558 (2020). DOI: https://doi.org/10.1680/jgele.20.00030